Evaluation of site-selective drug effects on GABA receptors using nanovesicle-carbon nanotube hybrid devices

Inkyoung Park, Inwoo Yang, Youngtak Cho, Yoonji Choi, Junghyun Shin, Shashank Shekhar, Seung Hwan Lee, Seunghun Hong

Evaluation of Site-Selective Drug Effects on GABA Receptors using Nanovesicle-Carbon Nanotube Hybrid Devices

*Inkyoung Park[‡1)], Inwoo Yang[‡2)], Youngtak Cho[1)], Yoonji Choi[1)], Junghyun Shin[1)], Shashank Shekhar[1)], Seung Hwan Lee[*2)], Seunghun Hong[*1)]*

[1)]Department of Physics and Astronomy, and the Institute of Applied Physics, Seoul National University, Seoul 08826, Republic of Korea

[2)]Department of Bionano Engineering, Center for Bionano Intelligence Education and Research, Hanyang University, Ansan, 15588, Republic of Korea

*Corresponding author.

Department of Physics and Astronomy, Seoul National University, Seoul 08826, Republic of Korea. *E-mail address:* seunghun@snu.ac.kr (S. Hong)

Department of Bionano Engineering, Center for Bionano Intelligence Education and Research, Hanyang University, Ansan, 15588, Republic of Korea. *E-mail address:* vincero78@gmail.com (S. H. Lee)

Abstract

Site-selective drug effects on the ion-channel activities of γ-aminobutyric acid type A ($GABA_A$) receptors are evaluated by using a nanovesicle-carbon nanotube hybrid device. Here, nanovesicles containing $GABA_A$ receptors are immobilized on the channel region of a carbon nanotube field-effect transistor. The receptor responses of this hybrid device to GABA are detected with a high sensitivity down to ~1 aM even in the presence of other neurotransmitters. Further, sensitivity differences between two $GABA_A$-receptor-subunit compositions of α5β2γ2 and α1β2γ2 are assessed by normalizing the dose-dependent responses obtained from these hybrid devices. Specifically, the GABA concentration that produces 50% of maximal response (EC_{50}) is obtained as ~10 pM for α5β2γ2 subunits and ~1 nM for α1β2γ2 subunits of $GABA_A$ receptor. Significantly, the potency profiles of both antagonist and agonist of $GABA_A$ receptor can be evaluated by analyzing EC_{50} values in the presence and absence of those drugs. A competitive antagonist increases the EC_{50} value of GABA by binding to the same site as GABA, while an allosteric agonist reduces it by binding to a different site. These results indicate that this hybrid device can be a powerful tool for the evaluation of candidate drug substances modulating GABA-mediated neurotransmission.

Keywords: hybrid nanodevice, carbon nanotube field-effect transistor, nanovesicle, GABA receptor, drug screening

1. Introduction

γ-aminobutyric acid type A ($GABA_A$) receptor is a ligand-gated chloride-ion channel that regulates neurotransmission in a central nervous system. A malfunction of this receptor leads to neurological disorders such as epilepsy, anxiety, and insomnia.(Chuang and Reddy, 2018; Jacob et al., 2008; Rudolph and Knoflach, 2011) Although benzodiazepines acting on $GABA_A$ receptors are widely-prescribed drugs for the treatment of these neurological disorders, they are used only limitedly due to side effects and addictiveness.(Fischer et al., 2011; Rudolph and Knoflach, 2011) A $GABA_A$ receptor assembles into a pentamer with combinations of numerous different subunits (α1–α6, β1–β3, γ1–γ3, δ, ε, π, θ, and ρ1–ρ3) and has multiple ligand-binding sites on the interfaces of five subunits.(Olsen and Sieghart, 2009) The limitation of benzodiazepines and the presence of versatile subunit combinations and multiple binding sites made $GABA_A$ receptors an important target for the development of new antipsychotic drugs. However, a lack of structural information on the binding sites has hindered the research on drug candidates which target $GABA_A$ receptors.(Zhu et al., 2018) Even though previous studies based on affinity labeling, mutagenesis, and a homology model have provided indirect information on the supposed binding sites of many drug candidates,(Chen et al., 2012; Desai et al., 2009; Ernst et al., 2003; Hosie et al., 2006; Padgett et al., 2007; Sieghart, 2015; Yip et al., 2013) it is still challenging to discover novel drugs acting on $GABA_A$ receptors. Recently, semisynthetic fluorescent biosensors for $GABA_A$-receptor ligands were developed by utilizing a fluorescence quenching and recovery system combined with affinity-based chemical labeling reagents.(Yamaura et al., 2016) These biosensors are suitable for high-throughput binding assays on drug candidates. However, ligand-binding assays cannot reveal the full potency profiles of drug candidates. Methods to detect ion-channel activities are essential to assess the efficacy of

drug candidates. Although a patch clamp technique has been widely utilized as a standard method for the study of ion-channel activities,(Knoflach et al., 2018; Verkman and Galietta, 2009) this conventional method has several drawbacks such as the need for advanced operating skill, labor-intensive procedures, and a high cost of automation.

Herein, we developed a carbon nanotube field-effect transistor (CNT-FET) hybridized with nanovesicles containing $GABA_A$ receptors to evaluate drug effects on ion-channel activities of $GABA_A$ receptors. In this work, CNT-FET devices were fabricated via microfabrication processes, (Kim et al., 2009; Kim et al., 2012; Lee et al., 2006; Park et al., 2012) and then nanovesicles containing $GABA_A$ receptors were immobilized on CNT channel regions coated with poly-D-lysine. GABA binding on $GABA_A$ receptors caused Cl^- influxes into nanovesicles and the consequent membrane hyperpolarization of nanovesicles, which resulted in the change of CNT channel conductance. Thus, we could electrically monitor GABA-mediated changes in transmembrane potential by using this nanovesicle-carbon nanotube hybrid device. This hybrid device allowed us to selectively detect GABA responses with a high sensitivity down to 1 aM even in the presence of other neurotransmitters, which indicated a better detection limit than those of conventional patch clamp techniques (~0.1 μM).(Hanson and Czajkowski, 2008; Knoflach et al., 2018; Wafford et al., 1993) By normalizing the GABA-dose-dependent responses of nanovesicle-CNT hybrid devices with $GABA_A$ receptors including two different subunit compositions of α5β2γ2 and α1β2γ2, we could show that the sensitivity of α5β3γ2 combination was higher than that of α1β2γ2 combination, which was in a good agreement with previously reported data.(Knoflach et al., 2018) The normalized responses of the hybrid devices were analyzed with the empirical Hill equation. Thereby, we could obtain the concentration of GABA that produces 50% of maximal response (EC_{50}) at ~10 pM for α5β2γ2 combination and ~1 nM for α1β2γ2

combination. Note that the estimated EC_{50} values were much smaller than previously reported values using live cells including $GABA_A$ receptors (10–100 μM).(Hanson and Czajkowski, 2008; Knoflach et al., 2018; Wafford et al., 1993) Presumably, the smaller size of nanovesicles than live cells resulted in a significant gating effect to CNT-FET transducers even with small amounts of Cl^- influxes. Significantly, we evaluated the effects of a competitive antagonist drug, bicuculline, and an allosteric agonist drug, etomidate. The EC_{50} values of GABA in the presence of *bicuculline* and *etomidate* in this hybrid assay were two orders of magnitude *higher* and *lower* than the EC_{50} values of GABA without drugs, respectively. Presumably, bicuculline bound to the same site as GABA, which competitively inhibited GABA-binding affinity. Etomidate bound to a different site from that of GABA, which enhanced GABA-evoked Cl^- influxes. These results show that this hybrid device can be used to evaluate the potency profiles of both antagonist and agonist drugs. This work could open up efficient ways to assess the effects of various drug candidates binding to $GABA_A$ receptors.

2. Materials and methods

2.1 Materials

Semiconducting 99% single-walled carbon nanotubes (swCNTs) were purchased from NanoIntegris, Inc. (Canada). γ-aminobutyric acid (GABA), bicuculine, etomidate, cytochalasin B, Dulbecco's phosphate buffered saline (DPBS), protease inhibitor cocktail, 1,2-dichlorobenzene, octadecyltrichlorosilane, and poly-D-lysine were purchased from Sigma Aldrich (USA). Dulbecco's Modified Eagle Medium (DMEM) and fetal bovine serum were purchased from Biowest (France). Penicillin-streptomycin serum was purchased from Gibco (USA). Lipofectamine 3000 was purchased from Invitrogen (USA).

2.2 Cell culture and nanovesicle production

Human embryonic kidney-293 (HEK-293) cells were cultured in DMEM with 10% fetal bovine serum and 1% penicillin-streptomycin at 37°C in a 5% CO_2 atmosphere. The cells were transfected with three kinds of pCMV6-Entry vectors containing γ-aminobutyric acid type A ($GABA_A$) receptor subunits (α1:β2:γ2=1:1:1 or α5:β2:γ2=1:1:1) by using Lipofectamine 3000 and additionally cultured for 48 h. Then, the HEK-293 cells containing $GABA_A$ receptors were harvested. Afterward, nanovesicles containing $GABA_A$ receptors were produced by 300 rpm agitation of the cells with 10 μg/mL cytochalasin B.(Lee et al., 2015; Pick et al., 2005; Shin et al., 2020) Cell debris was removed by centrifugation (1,000 G, 10 min). The nanovesicles were concentrated in DPBS containing protease inhibitor cocktail through centrifugation (15,000 G, 30 min). For control experiments, HEK-293 cells were transfected with mock pCMV6-Entry vector containing no receptor gene (empty vector) by using Lipofectamine 3000. Mock nanovesicles without $GABA_A$ receptors were produced from those parent cells via the same procedure described for nanovesicles containing $GABA_A$ receptors.

2.3 Western blot analysis

The cell and nanovesicle membranes containing $GABA_A$ receptors were disrupted via pulse sonication (2 s on/off cycles for 2 min). Then, the membrane fractions were collected by centrifugation (12,000 G, 30 min). Membrane proteins were isolated from the membrane fractions via polyacrylamide gel electrophoresis. For the detection of transfected $GABA_A$-receptor subunits among membrane proteins, a rabbit antibody to α1 subunit (Abcam, USA), a mouse antibody to β2 subunit (Sigma-Aldrich, USA), a rabbit antibody to γ2 subunit (Abcam, USA), and a mouse

antibody to α5 subunit (Santa Cruz Biotechnology, USA) were used as primary antibodies. As secondary antibodies, horseradish peroxidase (HRP)-conjugated antibodies (AbFrontier, Korea) were used. A western HRP substrate (Millipore, USA) was used to perform western blot.

2.4 Membrane potential assay

The cells or nanovesicles were incubated in a 96-well plate with a loading buffer containing a fluorescent dye of FLIPR membrane potential assay kits (Molecular Devices, USA) at 37℃ for 30 min. The changes in fluorescence intensity upon the addition of a GABA solution were observed by using a microplate leader (BMG Labtech, Germany).(Joesch et al., 2008; Liu et al., 2008) For the driving force of Cl^- movement toward the outside of membranes, a Cl^--free buffer was used to dissolve GABA.

2.5 CNT-FET device fabrication

To prepare a CNT suspension, a 0.05 mg/mL mixture of swCNTs and 1,2-dichlorobenzene was sonicated for 4 h. An octadecyltrichlorosilane monolayer with hydrophobic terminal groups was patterned on the SiO_2 substrate via photolithography as reported previously.(Jin et al., 2013) Then, the patterned substrate with the octadecyltrichlorosilane monolayer was immerged in the CNT suspension for 20 s. Then, the excess CNT suspension was washed out with 1,2-dichlorobenzene. Source, drain, and floating electrodes were fabricated on the substrate via photolithography and thermal evaporation. The floating electrodes were 10 μm wide and 200 μm long, and exposed CNT channels were 3 μm wide and 170 μm long. Except the channel region including the floating electrodes and exposed CNT channels, the surface of substrate was passivated with a photoresist

layer. In order to completely harden the passivation layer and to remove the chemicals that could damage biomolecules, the substrate with the passivation layer was incubated at 200℃ for 12 h.

2.7 Nanovesicle immobilization on a CNT-FET device

Poly-D-lysine was dissolved in distilled water, and the solution was diluted to prepare a 0.1 mg/mL working solution. Then, CNT channel regions of a CNT-FET device were covered with the working solution and incubated at 37℃ for 1 h, and the device was rinsed with water and dried at room temperature. After the nanovesicle production process, the concentration of total protein contained in the nanovesicle suspension was measured by a bicinchoninic acid assay kit (Pierce, IL, USA). Then, the nanovesicle suspension was diluted with a fresh DPBS solution to the same protein concentration at each device preparation step. Afterward, the diluted nanovesicle suspension was dropped onto the channel region, the device was incubated at 4℃ for 3 h, and loosely bound nanovesicles were removed by, at least, three times of DPBS washes before electrical measurements.

2.8 Electrical measurements

Before each electrical measurement, GABA solutions with various concentrations were prepared in a fresh DPBS solution via consecutive dilution steps. The nanovesicle-immobilized CNT-FET hybrid device was connected to probe electrodes of a semiconductor analyzer (Keithley 4200, Keithley Instruments, USA), and a fresh DPBS solution was placed on the channel region for physiological environments. A liquid gate bias was applied at a negative voltage around −0.5 V causing the highest reduction of source-drain currents, and a source-drain bias voltage was retained

at 0.2 V. Afterward, source-drain currents were measured upon the addition of GABA solutions with various concentrations.

2.9 SEM imaging of a nanovesicle-CNT hybrid device

The morphology of CNT networks and nanovesicles on a CNT-FET device was visualized by using a field-emission scanning electron microscope (FE-SEM) (SUPRA 55VP, Carl Zeiss, Germany). To maintain the structure of nanovesicles immobilized on the CNT channel region, membrane lipids were fixed with an OsO_4 solution before SEM imaging.

2.10 Size distribution and zeta potential of nanovesicles

The size distribution and zeta potential of nanovesicles were estimated by dynamic light scattering (DLS) and electrophoretic light scattering (ELS) measurements using Zetasizer Nano ZS90 (Malvern, Germany). Nanovesicles were dispersed in a DPBS solution at a concentration of 5 μg/mL. Disposable capillary cell (DTS1070, Malvern, Germany) with a sample volume of 80 μL was used for DLS and ELS measurements.

3. Results and discussion

3.1 Structure of a CNT-FET hybrid device with nanovesicles containing $GABA_A$ receptors

Figure 1 shows a schematic diagram describing a CNT-FET device hybridized with nanovesicles containing $GABA_A$ receptors. Detailed fabrication process is provided in Materials and Methods section. We also provided the schematic diagram showing the fabrication process of nanovesicle-CNT-FET hybrid device as a supplementary material (**Figure S1** in Supplementary Material). In this work, single-walled carbon nanotubes (swCNTs) with more than 99% of

semiconducting ones were selectively assembled in the channel regions on a SiO_2 substrate via a surface-directed assembly method. Then, source, drain, and floating electrodes were fabricated via photolithography and thermal evaporation.(Kim et al., 2009; Kim et al., 2012; Lee et al., 2006; Park et al., 2012) Afterward, except for floating electrodes and CNT channel region, source-drain electrodes were passivated with photoresist layers. Finally, nanovesicles containing $GABA_A$ receptors were immobilized on the channel regions coated with poly-D-lysine, a charge enhancer. The entire preparation steps of the nanovesicle-CNT-FET hybrid device were performed under the same conditions and protocol, resulting in identical dimensions of the floating electrodes and CNT channel region to which the nanovesicles were immobilized. When GABA molecules bound to their binding sites on pentameric $GABA_A$ receptors, Cl^- ions flowed into the nanovesicles through the ion channels of the receptors, which resulted in membrane hyperpolarization.(Rudolph and Knoflach, 2011) This led to the change of CNT channel conductance, allowing us to monitor GABA-mediated changes in transmembrane potential.

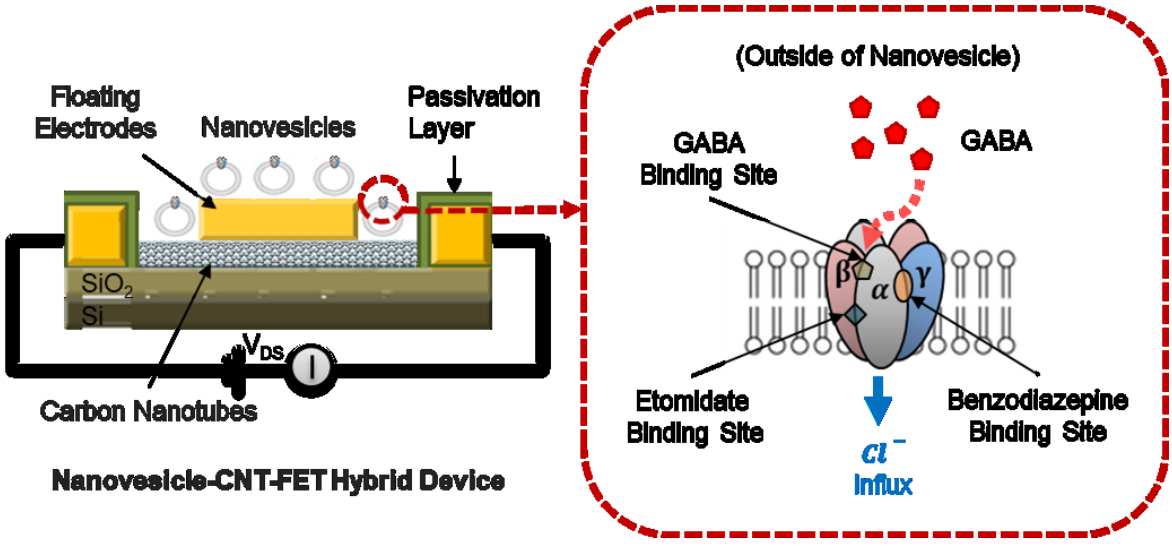

Figure 1. Schematic diagram depicting a nanovesicle-CNT-FET hybrid device. A CNT-FET device was fabricated via a surface-directed assembly method and microfabrication processes. Then, nanovesicles containing $GABA_A$ receptors composed of α5β2γ2 or α1β2γ2 subunits were immobilized on the CNT channel region coated with poly-D-lysine. GABA molecules bound to their binding sites on $GABA_A$ receptors, which resulted in $\boldsymbol{Cl^-}$ influxes into the membrane. A change in electric field caused by the $\boldsymbol{Cl^-}$ influxes induced a change in the CNT channel conductance.

3.2 Characterization of a CNT-FET hybrid device with nanovesicles containing $GABA_A$ receptors

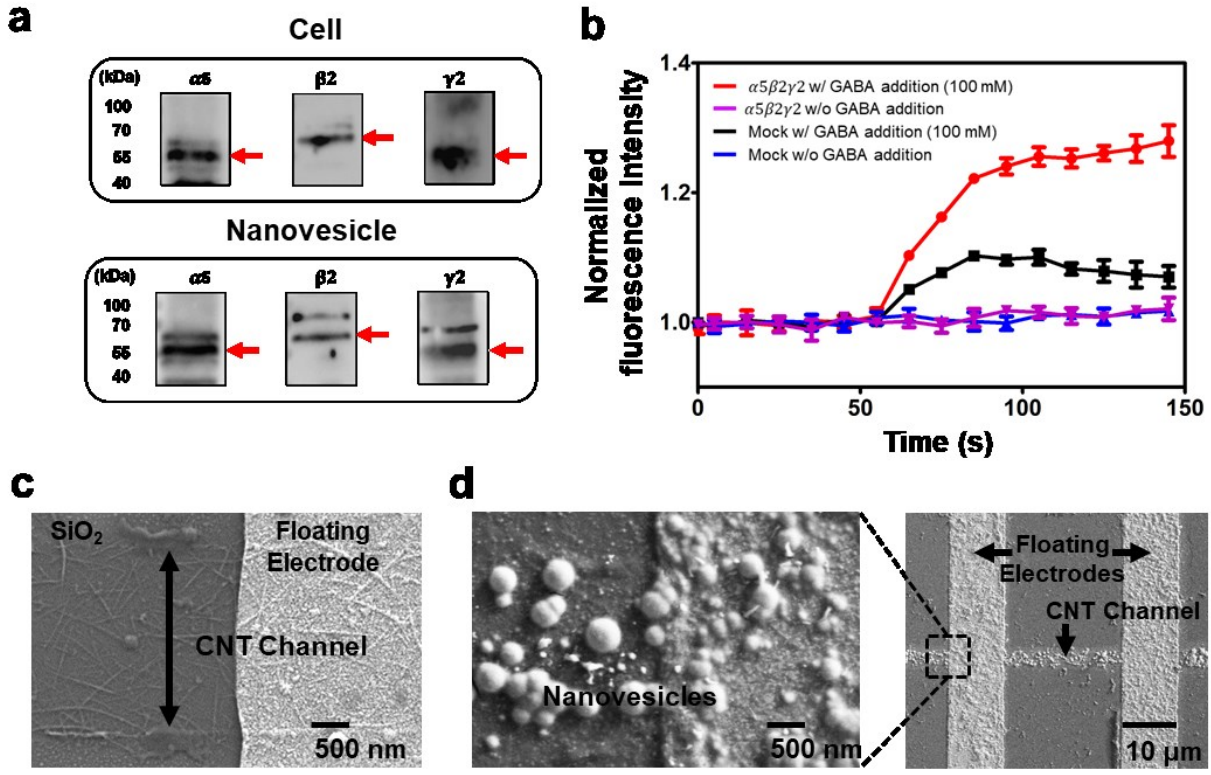

Figure 2. Expression of $GABA_A$ receptors in cell-derived nanovesicles and immobilization of nanovesicles on the channel region of CNT-FET. (a) Western blot analyses of α5, β2, and γ2 subunit proteins of $GABA_A$ receptor in HEK-293 cells and cell-derived nanovesicles. The red arrows indicate the specific bands corresponding to the molecular weights of α5, β2, and γ2 subunit proteins. (b) FLIPR membrane potential assay to investigate whether $GABA_A$ receptors maintained their functionalities when isolated into nanovesicles. The addition of a GABA solution (100 mM) led to much higher increase of a fluorescence intensity in the case of nanovesicles with $GABA_A$ receptors than those without $GABA_A$ receptors. The results are provided as mean ± SD. (c) FE-SEM image of bare CNT networks on a CNT-FET device. (d) FE-SEM images of nanovesicles immobilized on the channel region of CNT-FET. The diameters of nanovesicles immobilized on CNT networks and floating electrodes ranged from 200 nm to 400 nm.

The expression of $GABA_A$ receptors including two different subunit compositions of α5β2γ2 and α1β2γ2 in cell-derived nanovesicles were verified by Western blot analyses using antibodies against those subunit proteins (**Figure 2**a and **Figure S2**a in Supplementary Material). The red arrows in **Figure 2**a indicate the molecular weights of α5β2γ2 subunits, respectively. Specific bands from both cells and cell-derived nanovesicles correspond to α5β2γ2 subunits of $GABA_A$

receptor. These results show that each $GABA_A$-receptor subunit was expressed in cell-derived nanovesicles successfully. (Chen et al., 2012; Pettingill et al., 2015; Yamaura et al., 2016) In addition, the western blot analysis for HEK-293 cells transfected with mock pCMV6-Entry vector (empty vector) confirmed that those parent cells did not contain GABA-specific genes (**Figure S3** in Supplementary Material).

Figure 2b and **Figure S2**b (Supplementary Material) show the results of membrane potential assays, which was carried out to investigate whether GABA-activated membrane hyperpolarization could also occur in nanovesicles containing $GABA_A$-receptor subunits of α5β2γ2 and α1β2γ2, respectively. Here, nanovesicles with or without $GABA_A$ receptors were incubated in a well plate with a fluorescent dye of a commercially available kit for membrane potential assays. Then, real-time changes in fluorescence intensity were monitored by using a microplate leader. Here, we repeated the measurement by more than three times and provided a graph of mean values with their standard deviations as error bars. After the addition of a GABA solution (100 mM) into the well including nanovesicles with $GABA_A$ receptors, the fluorescence intensity (red lines) increased rapidly over the first twenty seconds and gradually saturated to a plateau phase. On the otherhand, in the control experiments without GABA addition, the fluorescence intensity did not change for both nanovesicles containing $GABA_A$ receptors and mock nanovesicles (purple and blue lines). It also should be mentioned that the addition of a GABA solution (100 mM) slightly increase the fluorescence intensity (black lines) in the case of mock nanovesicles without $GABA_A$ receptors. It was presumably due to the artifact signals caused by change in the concentration of extra-vesicle quencher included in the used assay kit to reduce background fluorescence.(May et al., 2010; Tay et al., 2019) Nevertheless, the fluorescence increase was much higher in nanovesicles with $GABA_A$ receptors than that by mock nanovesicles

beyond the range of error bars. These results show that the binding of GABA molecules to $GABA_A$ receptors caused Cl^- influxes into the nanovesicles containing $GABA_A$ receptors and the consequent membrane hyperpolarization. In these nanovesicle experiments, the recovery of fluorescence intensity to the baseline was not observed, possibly due to the lack of K^+/Cl^- cotransporters which are essential for the restoration of the Cl^- concentrations inside and outside the membrane.(Joesch et al., 2008; Liu et al., 2008) We could obtain a similar result with nanovesicles containing $GABA_A$-receptor subunits of α1β2γ2 (**Figure S2**b in Supplementary Material). These results suggest that $GABA_A$ receptors were successfully incorporated in a cell membrane and maintained their functionalities when isolated into nanovesicles.

Figure 2c and **Figure 2**d show the field-emission scanning electron microscopy (FE-SEM) images of CNT networks on a CNT-FET device and those of nanovesicles immobilized on the CNT channel region including floating electrodes, respectively. The detailed immobilization process using poly-D-lysine is provided in Methods section. To maintain the structure of nanovesicles during FE-SEM imaging, membrane lipids were fixed with an osmium tetroxide (OsO_4) solution. Also, OsO_4 molecules which bound onto phospholipid head groups created a high electron scattering rate without any metal layer coating. **Figure 2**d shows the uniform distribution of nanovesicles immobilized on swCNTs and floating electrodes. The diameters of nanovesicles ranged from 200 nm to 400 nm, which is consistent with the size distribution estimated by dynamic light scattering measurement of nanovesicles dispersed in a DPBS solution (**Figure S4** in Supplementary Material). Also, the zeta potential of nanovesicles was estimated to be −11 mV by electrophoretic light scattering. These results indicate that nanovesicles with a uniform size and a negative charge were successfully immobilized on a CNT channel region. It also should be mentioned that, though the number density of nanovesicles on the sensor surface could vary

slightly, we found that the sensor devices provided proper sensing signals with ~4.4 nanovesicles per square micrometer area. Considering the effective sensing area of ~$1.04 \times 10^{-8}\ m^2$ on our sensor chip (i.e., floating electrodes and CNT channel region), mean number of nanovesicles in a hybrid device was ~45,000.

3.3 GABA detection performance via nanovesicle-CNT-FET hybrid devices

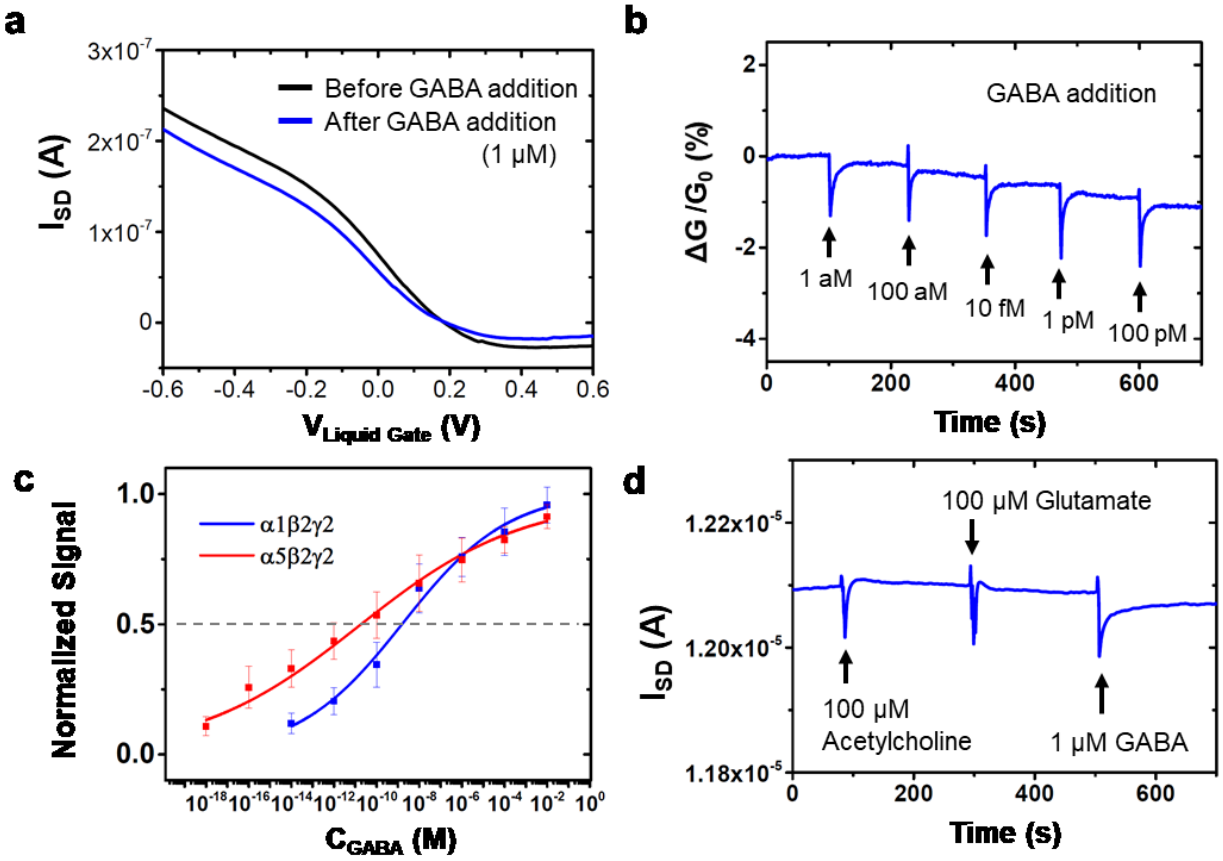

Figure 3. Characteristic responses of a nanovesicle-CNT-FET hybrid device to GABA. (a) Liquid gate profiles of a nanovesicle-CNT-FET hybrid device before and after a GABA introduction. (b) Real-time responses of a CNT-FET hybrid device at increasing GABA concentrations. The channel conductance decreased from the addition of 1 aM GABA solution. (c) GABA-dose-dependent responses of CNT-FET with $GABA_A$-receptor subunits of α5β2γ2 and α1β2γ2. The signals were obtained by normalizing |ΔG/G0| with respect to $|\Delta G/G0|_{max}$. The measurements were repeatedly carried out with multiple devices to obtain average values and standard deviations. The normalized signals were fitted by the Hill equation, with EC_{50} values as ~10 pM for the α5β2γ2 combination and ~1 nM for the α1β2γ2 combination. (d) Real-time responses of a nanovesicle-CNT-FET hybrid device to various neurotransmitters. A drastic decrease in current was occurred only with a GABA addition.

Figure 3a shows the liquid gate profiles of a nanovesicle-CNT-FET hybrid device before and after a GABA introduction. After the nanovesicle immobilization process, a fresh DPBS solution was placed on the channel region of a hybrid device. To investigate liquid gate profiles of the hybrid device, a liquid gate bias (V_{LG}) was applied into a DPBS solution above the nanovesicle-immobilized channel region via an Ag/AgCl electrode. The source-drain currents (I_{SD}) were measured while V_{LG} was swept from −0.6 V to 0.6 V with a source-drain bias of 0.2 V. The source-drain currents decreased with increasing gate voltages, indicating a *p-type* semiconducting property. Note that, after 1 μM GABA addition to this hybrid device, the source-drain currents were decreased at a negative gate voltage region. This result could be explained by the combination of electrostatic gating and Schottky barrier effects. GABA-evoked Cl^- influxes into nanovesicles resulted in more uncompensated positive charges outside the membrane and more uncompensated negative charges inside the membrane, which is called hyperpolarization. The uncompensated positive charges which were physically located in the immediate vicinity of the membrane induced electrostatic gating effects onto CNT networks and modulated local work function of floating electrodes and the consequent band alignment. Presumably, the obserbed decrease of source-drain currents at a negative gate voltage region arose from the combination of a curve shift toward negative gate voltages and a slope reduction. The curve shift was attributed to electrostatic gating effects of the positive charges onto CNT networks, and the slope reduction was due to the Schottky barrier height modulation caused by changes in local work function of floating electrodes.(Heller et al., 2008; Minot et al., 2007) These results imply that GABA-evoked membrane hyperpolarization would lead to the decrease of CNT channel conductance with a negative liquid gate bias.

Figure 3b shows the real-time responses of a CNT-FET device hybridized with nanovesicles containing $GABA_A$-receptor subunits of α5β2γ2 to GABA solutions. For each electrical measurement, an 18 μL droplet of fresh DPBS solution was placed on the channel region of a hybrid device. Then, source-drain currents were measured in real-time while adding GABA solutions. First, 2 μL of GABA solution with 10^{-17} M concentration was added onto the buffer region, resulting in 20 μL of GABA solution with 10^{-18} M concentration. Then, GABA solutions with increasing concentrations by the factor of 100 were consecutively added each time. The added volumes of GABA solutions with increasing concentrations were calculated by considering the increased total volume of buffer. During the measurement, a liquid gate bias was used at a negative value around −0.5 V for the largest change of source-drain currents, and a source-drain bias was retained at 0.2 V. Here, the detection signal was defined as the relative change of CNT channel conductance ($\Delta G/G_0$) at a given GABA concentration. The introduction of GABA solutions first led to a sharp spike-like fluctuation, and then the sensor signals were stabilized to the decreased values of $\Delta G/G_0$ with a dose-dependent manner. The spike noise was probably due to the physical vibration of the sample solution on the device during the introduction of GABA solutions as reported previously.(Yang et al., 2017) It should be mentioned that the detachment of nanovesicles during the measurement could induce a sharp decrease in electric currents over orders of magnitude, which allowed us to rule out possible artifacts in our sensor signals. To prevent the detachment, GABA solutions with increasing concentration were softly added onto the channel region during experiments. Each stabilized value of $\Delta G/G_0$ at a given GABA concentration represented an equilibrium state established between the concentrations of receptor-bound and free GABA molecules. Significantly, the detection signals decreased from the addition of 1 aM GABA solution. Note that a recent study using an automated patch clamp system with live cells including $GABA_A$

receptors showed the limit of detection (LOD) down to 0.1 μM GABA concentration,(Knoflach et al., 2018) indicating a high sensitivity of this hybrid device compared with previous methods.(Hanson and Czajkowski, 2008; Knoflach et al., 2018; Wafford et al., 1993) The high sensitivity of our hybrid device can be attributed to the smaller size of nanovesicles (*diameter* ~300 nm) than those of an individual cell used in previous methods, a large number of nanovesicles on a hybrid device (# ~45,000), and the high signal transduction efficiency of CNT-FET device. On the other hand, conventional methods such as a patch clamp technique usually relied on a measurement on a rather large individual cell using metal electrodes or pipettes. Considering the number of nanovesicles on a hybrid device (# ~45,000) and the number of GABA molecules included in 20 μL of 1 aM GABA solution (# ~12), the number of nanovesicles per GABA molecule in 20 μL GABA solution of 1 aM was ~3,750 in our hybrid device. It also should be mentioned that the recovery of source-drain currents was not observed in our measurements using this nanovesicle-CNT hybrid device. Presumably, K^+/Cl^- cotransporters did not exist in the nanovesicles, and, thus, Cl^- concentration in nanovesicles couldn't be restored, which was in agreement with the results of membrane potential assays in **Figure 2**b. We could obtain a similar response with a CNT-FET device hybridized with nanovesicles containing $GABA_A$-receptor subunits of α1β2γ2 (**Figure S5** in Supplementary Material). Also, we performed a control experiment using a sensor device with mock nanovesicles and obtained null responses (**Figure S6** in Supplementary Material). It supports that our sensor signals were originated from the activities of $GABA_A$ receptors on the nanovesicles. These results show that nanovesicle-CNT-FET hybrid devices could allow us to detect GABA-evoked ion-channel activities in nanovesicles with a high sensitivity and without a fast desensitization.

Figure 3c shows the normalized dose-dependent responses of CNT-FET devices hybridized with nanovesicles containing $GABA_A$-receptor subunits of α5β2γ2 and α1β2γ2 to GABA solutions with increasing concentrations. In our hybrid devices, the dimensions of sensing area (i.e., floating electrodes and CNT channel region) were identical. Nevertheless, the expression level of $GABA_A$ receptors, the size distribution of nanovesicles, and the number density of nanovesicles on the sensing area could vary slightly in each device. These variations could result in a different maximal amplitude of detection signal for each device. Thus, the relative conductance changes ($|\Delta G/G_0|$) of devices were re-normalized with respect to maximal values ($|\Delta G/G_0|_{max}$). The normalized signals at a given GABA concentration were measured with multiple devices to acquire average values and standard deviations. The signals increased with increasing GABA concentrations and saturated at a high concentration condition. The LOD of our device was 1 aM of GABA concentration and its dynamic range was from 1 aM to 10 mM. The responses of nanovesicle-CNT-FET hybrid devices with two different subunit compositions indicated that the sensitivity of α5β2γ2 combination was higher than that of α1β2γ2 combination. This result was consistent with previously reported data.(Knoflach et al., 2018) It was presumably due to the higher GABA affinity of α5-β2 interfaces than that of α1-β2 interfaces, since GABA-binding sites were supposed to locate on α-β interfaces.(Rudolph and Knoflach, 2011; Yamaura et al., 2016; Zhu et al., 2018) Meanwhile, various methods for detecting GABA molecules have been reported so far.(El-Said et al., 2020; Hossain et al., 2018; Huang et al., 2017; Lee et al., 2019; Monge-Acuña and Fornaguera-Trías, 2009; Prasad et al., 2013; Wang and Muthuswamy, 2008) The comparison of different methods using various recognition elements for GABA detection is presented in **Figure S7** (Supplementary Material). Our sensor device based on $GABA_A$ receptors exhibited a higher sensitivity than previous methods based on other recognition elements. Another advantage can be

that our device can be utilized to measure GABA-evoked ion-channel activities of $GABA_A$ receptors, which is the main purpose of our works. In addition, our hybrid device could be used to evaluate GABA sensitivities of $GABA_A$ receptors with two different subunit compositions in terms of ion-channel activity. On the other hand, previous methods based on more stable recognition elements like polymer structures should be advantageous over our sensors in terms of portability.

The dose-dependent responses of CNT-FET hybrid devices could be analyzed by the empirical Hill equation.(Neubig et al., 2003) Previous works reported that the normalized dose-dependent responses *N* of a CNT-FET based biosensor could be characterized as follows:(Pham Ba et al., 2017)

$$\mathrm{N} = \frac{|\Delta G/G_0|}{|\Delta G/G_0|_{max}} = \frac{C^n}{C^n + {EC_{50}}^n} \quad (1)$$

where *C*, EC_{50} and *n* are *GABA concentration*, the *GABA concentration producing 50% of maximal response*, and a *Hill coefficient*, respectively. Fitting the normalized dose-dependent responses with Equation (1), we could estimate the EC_{50} values (means $\pm$ standard errors) as 14.4 ± 21.7 pM for α5β2γ2 subunits of $GABA_A$ receptor and 1.2 ± 1.0 nM for α1β2γ2 subunits of $GABA_A$ receptor. The calculated EC_{50} values were much smaller than previously reported values (10–100 μM) measured by conventional patch clamp techniques and live cells with $GABA_A$ receptors.(Hanson and Czajkowski, 2008; Knoflach et al., 2018; Wafford et al., 1993) Note that, the potency of an agonist is dependent on experimental conditions such as used cells, a level of receptor expression, a type of measurement methods, and a signal transduction efficiency.(Neubig et al., 2003) In this work, since nanovesicles were much smaller than live cells, small amounts of Cl^- influxes into the nanovesicles could considerably enhance their electrical potential, which resulted in a remarkable gating effect on the CNT-FET transducers. Similar results have also been reported previously in other nanovesicle-carbon nanotube hybrid devices.(Jin et al., 2013) The

results show that one could achieve enhanced sensitivities and reduced EC_{50} values of ligands in this nanovesicle-CNT-FET hybrid assay. Using this hybrid device, the potency profiles of various drugs could be evaluated by comparing the EC_{50} values of GABA in the presence and absence of drugs.

Figure 3d shows the real-time response of a nanovesicle-CNT-FET hybrid device to different neurotransmitters. Here, we successively added the 100 μM solutions of acetylcholine, glutamate, and 1 μM GABA solution onto the hybrid device during electrical measurements. Acetylcholine and glutamate are major neurotransmitters acting on different receptors from GABA receptors. A distinct decrease in electric currents was observed only with a GABA addition. These results clearly show that the CNT-FET hybrid device could discriminate GABA even in the presence of other neurotransmitters with a high selectivity.

3.4 Evaluation of site-selective drug effects on $GABA_A$-receptor activities via nanovesicle-CNT-FET hybrid devices

Further, we extended the panel of selectivity to interfering molecules with GABA activities beyond different neurotransmitters. To date, a number of GABA analogues and $GABA_A$-receptor ligands that bind to various sites on pentameric $GABA_A$ receptor and modulate GABA activities are known and still being discovered. To demonstrate that our hybrid device can discriminate the site-selective effect of ligands, we chose a competitive antagonist that binds to the same site as GABA and an allosteric agonist that binds to a different site. **Figure 4**a illustrates the schematic diagram depicting the binding sites of two different drugs which modulate GABA-mediated Cl^- influxes. In this work, we evaluated the effects of *bicuculline* and *etomidate* which were known as *a competitive antagonist* and *an allosteric agonist* of $GABA_A$ receptor, respectively.(Belelli et al.,

1997; Horne et al., 1992; Yamaura et al., 2016; Zhu et al., 2018) Bicuculline competitively binds to the same site as GABA, which leads to the inhibition of GABA binding to $GABA_A$ receptors. On the other hand, etomidate is known to bind to a different site, and the binding of etomidate actually enhances GABA-evoked Cl^- influxes. Since the modulated amounts of Cl^- influxes resulted in the conductance changes of CNT channels, the potency profiles of different drugs acting on $GABA_A$ receptors could be electrically assessed by using our hybrid devices.

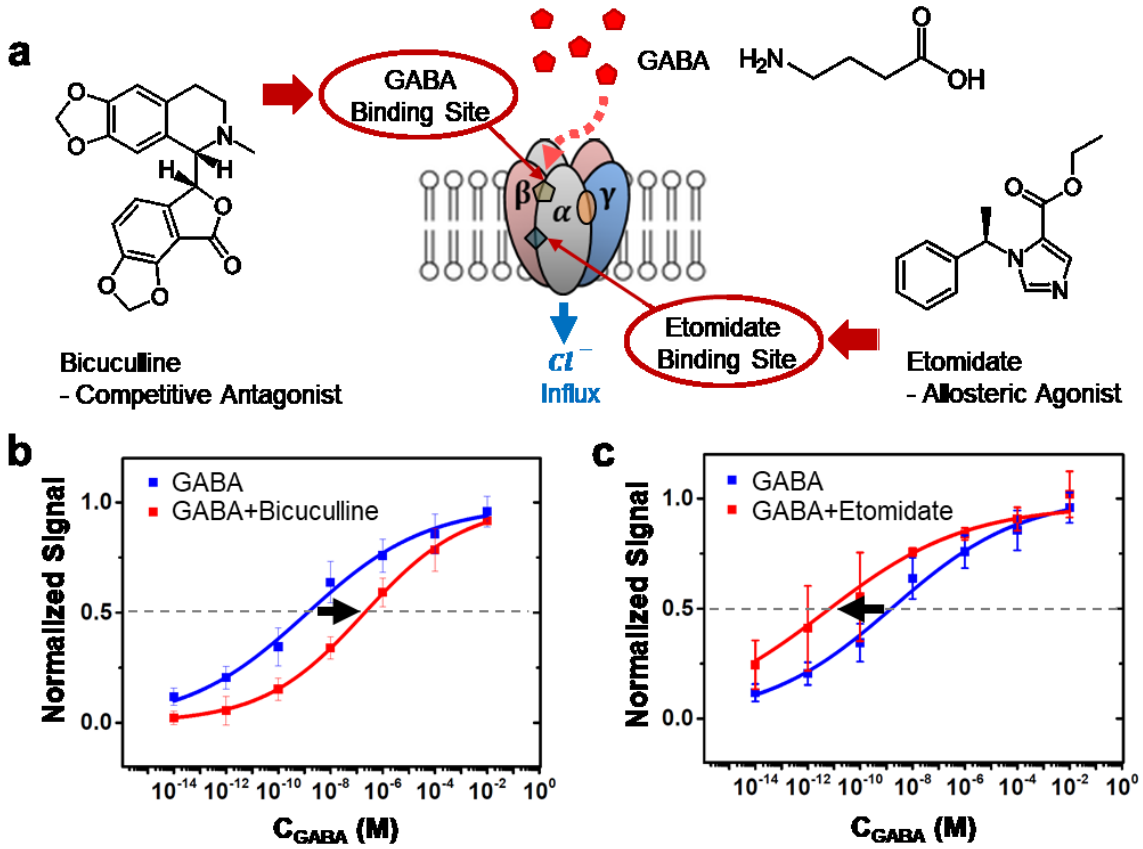

Figure 4. Evaluation of site-selective drug effects on ion-channel activities of $GABA_A$ receptors. (a) Schematic depicting the binding sites of two different drugs modulating GABA-evoked $\boldsymbol{Cl^-}$ influxes. (b) Normalized dose-dependent responses of CNT-FET hybrid devices to GABA in the presence and absence of competitive antagonist, bicuculine with 100 μM. The EC_{50} value was shifted to higher GABA concentration by two orders of magnitude in the presence of bicuculine. (c) Normalized dose-dependent responses of CNT-FET hybrid devices to GABA in the presence and absence of allosteric agonist, etomidate with 100 μM. The EC_{50} value was shifted to lower GABA concentration by two orders of magnitude in the presence of etomidate. (b, c) The signals were obtained by normalizing $|\Delta G/G0|$ with respect to $|\Delta G/G0|_{max}$. The normalized signals were fitted by the Hill equation.

Figure 4b shows the normalized dose-dependent responses of CNT-FET hybrid devices with nanovesicles containing $GABA_A$-receptor subunits of α1β2γ2 to GABA with and without

bicuculine. Here, nanovesicles immobilized on CNT channel regions were incubated with a DPBS solution with or without 100 μM bicuculine. Then, the responses of individual hybrid devices to the addition of GABA solutions with different concentrations were measured. Each data point was obtained by normalizing $|\Delta G/G_0|$ with respect to $|\Delta G/G_0|_{max}$, and the normalized responses of the hybrid devices were analyzed by fitting them with the Hill equation. The normalized signals in the presence of bicuculine were shifted toward a high concentration region, which was consistent with previously reported data.(Horne et al., 1992; Zhu et al., 2018) The EC_{50} value of GABA in the presence of bicuculine estimated in our nanovesicle-CNT-FET hybrid assay was 190.0 ± 35.7 nM, which was two orders of magnitude higher than that of GABA without bicuculine (1.2 ± 1.0 nM). This result shows that the competitive binding of bicuculine to GABA-binding sites dramatically reduced the affinity between GABA and $GABA_A$ receptor.

Figure 4c shows the normalized dose-dependent responses of CNT-FET hybrid devices with nanovesicles containing $GABA_A$-receptor subunits α1β2γ2 to GABA in the presence and absence of etomidate. In this case, after nanovesicles on CNT channel regions were incubated with a buffer solution with or without 100 μM etomidate, the responses of the devices to GABA addition were measured. Each data point at a given concentration was obtained by normalizing $|\Delta G/G_0|$ with respect to $|\Delta G/G_0|_{max}$, and the normalized responses were analyzed by the Hill equation. In the presence of etomidate, the normalized signals were shifted toward a low concentration region, in agreement with previous studies on allosteric agonists.(Belelli et al., 1997; Yamaura et al., 2016) The EC_{50} value of GABA in the presence of etomidate estimated in this hybrid assay was 4.7 ± 3.8 pM, which was two orders of magnitude lower than that of GABA without etomidate (1.2 ± 1.0 nM). This result shows that the simultaneous binding of GABA and etomidate onto $GABA_A$

receptors significantly enhanced Cl^- influxes into nanovesicles. It should be noted that since this hybrid device could successfully evaluate the potency profiles of both antagonist and agonist, it can be a powerful method for the screening of new drugs to modulate ion-channel activities.

4. Conclusion

We have successfully evaluated the potency profiles of GABA-related drugs in a site-selective manner by using nanovesicle-CNT-FET hybrid devices containing $GABA_A$ receptors. Here, the functional activities of $GABA_A$ receptors incorporated in nanovesicles were verified via a membrane potential assay. Then, the nanovesicles were immobilized on the channel region of CNT-FET devices. Using this hybrid device, we could detect GABA responses with a high sensitivity down to 1 aM even in the presence of other neurotransmitters. Further, we could evaluate the sensitivities of different subunit combinations by normalizing the dose-dependent responses of the hybrid devices with $GABA_A$ receptors of two different subunit compositions. By fitting the dose-dependent responses of the hybrid devices with the Hill equation, we could obtain the EC_{50} value of GABA as ~10 pM for α5β2γ2 subunits and ~1 nM for α1β2γ2 subunits. Importantly, we have demonstrated both antagonism and agonism of $GABA_A$ receptor by comparing the EC_{50} values of GABA in the presence and absence of drugs. In the presence of competitive antagonists, the EC_{50} value was shifted to a high GABA concentration region by two orders of magnitude. On the other hand, in the presence of allosteric agonists, the EC_{50} value was shifted to a low GABA concentration region by similar orders. Since this hybrid device allows one to evaluate the potency profiles of drug candidates, it can be a powerful tool for pharmacological research and drug screening applications.

Author contributions

‡ **Inkyoung Park** and **Inwoo Yang** contributed equally to this work. **Inkyoung Park** prepared devices and performed a sensor measurement. **Inwoo Yang** prepared receptors and nanovesicles. **Youngtak Cho**, **Yoonji Choi**, **Junghyun Shin**, and **Shashank Shekhar** contributed to device preparation and data analyses. **Inkyoung Park**, **Inwoo Yang**, **Seung Hwan Lee**, and **Seunghun Hong** conceived key ideas. All authors participated in the preparation of the manuscript.

Declaration of interests

The authors declare that they have no known competing financial interests or personal relationships that could have appeared to influence the work reported in this paper.

Acknowledgments

This work was supported by the National Research Foundation of Korea (NRF) funded by the Ministry of Science and ICT (MSIT) of Korea (No. 2013M3A6B2078961, 2018R1C1B5085757 and 2020R1A2B5B02002152) and the Ministry of Education (No. 2018R1A6A1A03024231). S. Hong would like to acknowledge the support from the Ministry of Trade, Industry & Energy (MOTIE, Korea) (No. 20012390), Samsung Electronics Co. Ltd. (No. 201209-07908-01), and the European Research Council (ERC) under the European Union's Horizon 2020 programme (grant agreement no. 682286).

References

Belelli, D., Lambert, J.J., Peters, J.A., Wafford, K., Whiting, P.J., 1997. Proceedings of the National Academy of Sciences 94, 11031–11036.. doi:10.1073/pnas.94.20.11031

Chen, Z.-W., Manion, B., Townsend, R.R., Reichert, D.E., Covey, D.F., Steinbach, J.H., Sieghart, W., Fuchs, K., Evers, A.S., 2012. Molecular Pharmacology 82, 408–419.. doi:10.1124/mol.112.078410

Chuang, S.-H., Reddy, D.S., 2018. Journal of Pharmacology and Experimental Therapeutics 364, 180–197.. doi:10.1124/jpet.117.244673

Desai, R., Ruesch, D., Forman S.A., 2009. Anesthesiology 111, 774–784.. doi:10.1097/aln.0b013e3181b55fae

El-Said, W.A., Alshitari, W., Choi, J.-W., 2020. Spectrochimica Acta Part A: Molecular and Biomolecular Spectroscopy 229, 117890.. doi:10.1016/j.saa.2019.117890

Ernst, M., Brauchart, D., Boresch, S., Sieghart, W., 2003. Neuroscience 119, 933–943.. doi:10.1016/s0306-4522(03)00288-4

Fischer, B.D., Atack, J.R., Platt, D.M., Reynolds, D.S., Dawson, G.R., Rowlett, J.K., 2011. Psychopharmacology 215, 311–319.. doi:10.1007/s00213-010-2142-y

Hanson, S.M., Czajkowski, C., 2008. The Journal of Neuroscience 28, 3490–3499.. doi:10.1523/jneurosci.5727-07.2008

Heller, I., Janssens, A.M., Männik, J., Minot, E.D., Lemay, S.G., Dekker, C., 2008. Nano Letters 8, 591–595.. doi:10.1021/nl072996i

Horne, A.L., Hadingham, K.L., Macaulay, A.J., Whiting, P., Kemp, J.A., 1992. British Journal of Pharmacology 107, 732–737.. doi:10.1111/j.1476-5381.1992.tb14515.x

Hosie, A.M., Wilkins, M.E., Da Silva, H.M.A., Smart, T.G., 2006. Nature 444, 486–489.. doi:10.1038/nature05324

Hossain, I., Tan, C., Doughty, P. T., Dutta, G., Murray, T. A., Siddiqui, S., Iasemidis, L., Arumugam, P. U., 2018. Frontiers in neuroscience 12, 500.. doi:10.3389/fnins.2018.00500

Huang, Y., Ding, M., Guo, T., Hu, D., Cao, Y., Jin, L., Guan, B.-O., 2017. Nanoscale 9, 14929–14936.. doi:10.1039/c7nr05032a

Jacob, T.C., Moss, S.J., Jurd, R., 2008. Nature Reviews Neuroscience 9, 331–343.. doi:10.1038/nrn2370

Jin, H.J., An, J.M., Park, J., Moon, S.J., Hong, S., 2013. Biosensors and Bioelectronics 49, 86–91.. doi:10.1016/j.bios.2013.04.045

Joesch, C., Guevarra, E., Parel, S.P., Bergner, A., Zbinden, P., Konrad, D., Albrecht, H., 2008. Journal of Biomolecular Screening 13, 218–228.. doi:10.1177/1087057108315036

Kim, B., Lee, J., Namgung, S., Kim, J., Park, J.Y., Lee, M.-S., Hong, S., 2012. Sensors and Actuators B: Chemical 169, 182–187.. doi:10.1016/j.snb.2012.04.063

Kim, T.H., Lee, S.H., Lee, J., Song, H.S., Oh, E.H., Park, T.H., Hong, S., 2009. Advanced Materials 21, 91–94.. doi:10.1002/adma.200801435

Knoflach, F., Hernandez, M.-C., Bertrand, D., 2018. Journal of Visualized Experiments.. doi:10.3791/57842

Lee, J.-H., Chae, E.-J., Park, S.-J., Choi, J.-W., 2019. Nano Convergence 6.. doi:10.1186/s40580-019-0184-3

Lee, M., Im, J., Lee, B.Y., Myung, S., Kang, J., Huang, L., Kwon, Y.-K., Hong, S., 2006. Nature Nanotechnology 1, 66–71.. doi:10.1038/nnano.2006.46

Lee, M., Jung, J.W., Kim, D., Ahn, Y.-J., Hong, S., Kwon, H.W., 2015. ACS Nano 9, 11728–11736.. doi:10.1021/acsnano.5b03031

Liu, J., Chen, T., Norris, T., Knappenberger, K., Huston, J., Wood, M., Bostwick, R., 2008. Assay and drug development technologies 6, 781-786.. doi: 10.1089/adt.2008.161

May, L.T., Briddon, S.J., Hill, S.J., 2010. Molecular Pharmacology 77, 678–686.. doi:10.1124/mol.109.063065

Minot, E.D., Janssens, A.M., Heller, I., Heering, H.A., Dekker, C., Lemay, S.G., 2007. Applied Physics Letters 91, 093507.. doi:10.1063/1.2775090

Monge-Acuña, A.A., Fornaguera-Trías, J., 2009. Journal of Neuroscience Methods 183, 176–181.. doi:10.1016/j.jneumeth.2009.06.042

Neubig, R.R., Spedding, M., Kenakin, T., Christopoulos, A., 2003. Pharmacological Reviews 55, 597–606.. doi:10.1124/pr.55.4.4

Olsen, R.W., Sieghart, W., 2009. Neuropharmacology 56, 141–148.. doi:10.1016/j.neuropharm.2008.07.045

Padgett, C.L., Hanek, A.P., Lester, H.A., Dougherty, D.A., Lummis, S.C.R., 2007. The Journal of Neuroscience 27, 886–892.. doi:10.1523/jneurosci.4791-06.2007

Park, J., Lim, J.H., Jin, H.J., Namgung, S., Lee, S.H., Park, T.H., Hong, S., 2012. The Analyst 137, 3249.. doi:10.1039/c2an16274a

Pettingill, P., Kramer, H.B., Coebergh, J.A., Pettingill, R., Maxwell, S., Nibber, A., Malaspina, A., Jacob, A., Irani, S.R., Buckley, C., Beeson, D., Lang, B., Waters, P., Vincent, A., 2015. Neurology 84, 1233–1241.. doi:10.1212/wnl.0000000000001326

Pham Ba, V.A., Cho, D.-G., Kim, D., Yoo, H., Ta, V.-T., Hong, S., 2017. Biosensors and Bioelectronics 94, 707–713.. doi:10.1016/j.bios.2017.03.063

Pick, H., Schmid, E.L., Tairi, A.-P., Ilegems, E., Hovius, R., Vogel, H., 2005. Journal of the American Chemical Society 127, 2908–2912.. doi:10.1021/ja044605x

Prasad, B.B., Prasad, A., Tiwari, M.P., 2013. Electrochimica Acta 102, 400–408.. doi:10.1016/j.electacta.2013.04.043

Rudolph, U., Knoflach, F., 2011. Nature Reviews Drug Discovery 10, 685–697.. doi:10.1038/nrd3502

Shin, N., Lee, S.H., Cho, Y., Park, T.H., Hong, S., 2020. Small 16, 2001469.. doi:10.1002/smll.202001469

Sieghart, W., 2015. in: Rudolph, U. (Ed.), Advances in Pharmacology. Academic Press, pp. 53-96.. doi:10.1016/bs.apha.2014.10.002

Tay, B., Stewart, T.A., Davis, F.M., Deuis, J.R., Vetter, I., 2019. PLOS ONE 14, e0213751.. doi:10.1371/journal.pone.0213751

Verkman, A.S., Galietta, L.J.V., 2009. Nature Reviews Drug Discovery 8, 153–171.. doi:10.1038/nrd2780

Wafford, K. A., Whiting, P. J., Kemp, J. A., 1993. Molecular Pharmacology 43, 240-244.

Wang, T., Muthuswamy, J., 2008. Analytical Chemistry 80, 8576–8582.. doi:10.1021/ac801463a

Yamaura, K., Kiyonaka, S., Numata, T., Inoue, R., Hamachi, I., 2016. Nature Chemical Biology 12, 822–830.. doi:10.1038/nchembio.2150

Yang, H., Kim, D., Kim, J., Moon, D., Song, H.S., Lee, M., Hong, S., Park, T.H., 2017. ACS Nano 11, 11847–11855.. doi:10.1021/acsnano.7b04992

Yip, G.M.S., Chen, Z.-W., Edge, C.J., Smith, E.H., Dickinson, R., Hohenester, E., Townsend, R.R., Fuchs, K., Sieghart, W., Evers, A.S., Franks, N.P., 2013. Nature Chemical Biology 9, 715–720.. doi:10.1038/nchembio.1340

Zhu, S., Noviello, C.M., Teng, J., Walsh, R.M., Kim, J.J., Hibbs, R.E., 2018. Nature 559, 67–72.. doi:10.1038/s41586-018-0255-3

Supplementary Material

Evaluation of Site-Selective Drug Effects on GABA Receptors using Nanovesicle-Carbon Nanotube Hybrid Devices

Inkyoung Park[‡1)], *Inwoo Yang*[‡2)], *Youngtak Cho*[1)], *Yoonji Choi*[1)], *Junghyun Shin*[1)], *Shashank Shekhar*[1)], *Seung Hwan Lee*[*2)], *Seunghun Hong*[*1)]

[1)]Department of Physics and Astronomy, Seoul National University, Seoul 08826, Republic of Korea

[2)]Department of Bionano Engineering, Center for Bionano Intelligence Education and Research, Hanyang University, Ansan, 15588, Republic of Korea

*Corresponding author. *E-mail:* seunghun@snu.ac.kr (S. Hong) vincero78@gmail.com (S. H. Lee)

Figure S1

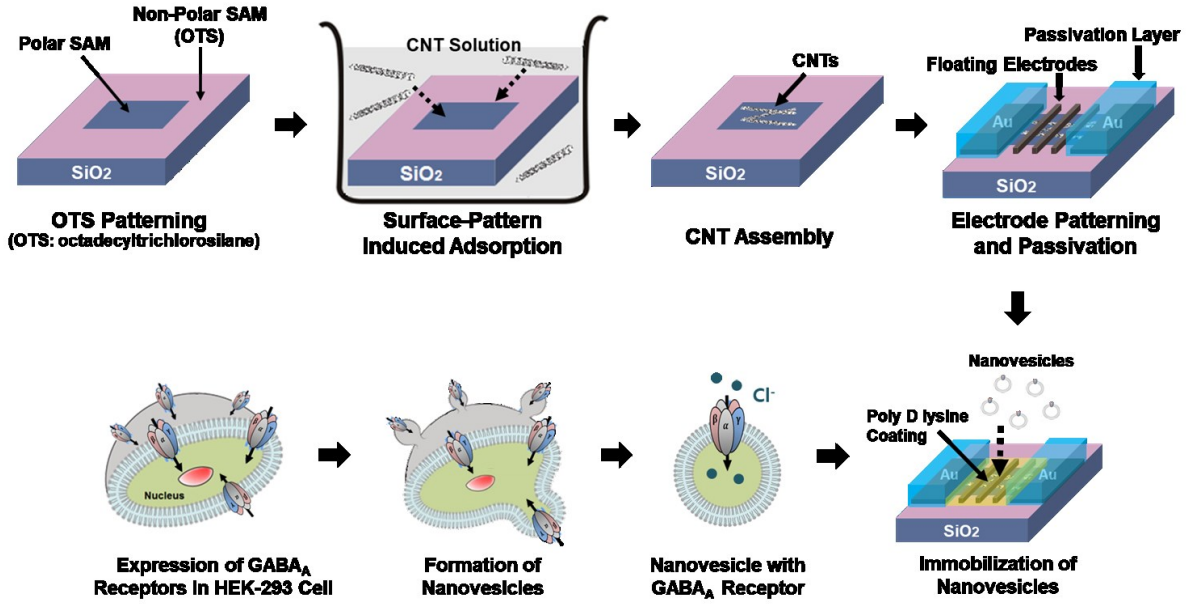

Figure S1. Schematic diagram showing the fabrication of nanovesicle-CNT-FET hybrid device.

Figure S2

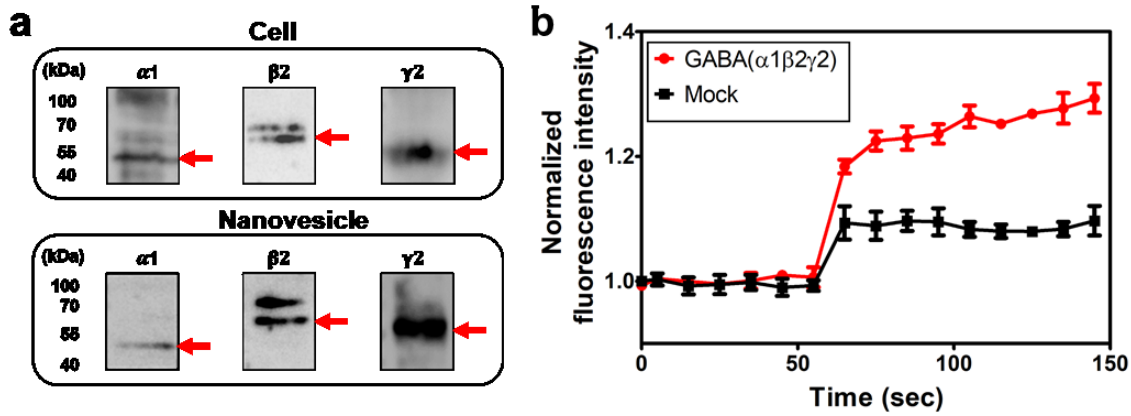

Figure S2. Expression of $GABA_A$-receptor subunits of α1β2γ2 in cell-derived nanovesicles. (a) Western blot analyses of $GABA_A$-receptor subunits of α1β2γ2 expression in HEK-293 cells and cell-derived nanovesicles. The red arrows indicate the specific bands corresponding to the molecular weights of α1, β2, and γ2 subunit proteins. (b) FLIPR membrane potential assay to investigate whether $GABA_A$-receptor subunits of α1β2γ2 maintained their functionalities when isolated into nanovesicles. The addition of a GABA solution (100 mM) resulted in much larger increase of a fluorescence intensity in the case of nanovesicles with $GABA_A$ receptors than those without $GABA_A$ receptors. The results are provided as mean ± SD.

Figure S3

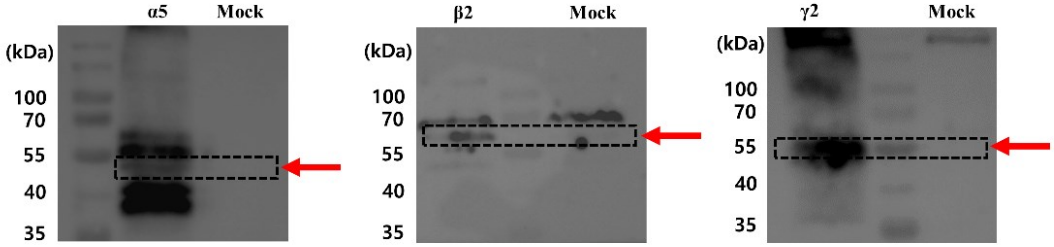

Figure S3. Western blot analyses of α5, β2, and γ2 subunit proteins of $GABA_A$ receptor in HEK-293 cells. For control experiments, HEK-293 cells were further transfected with mock pCMV6-Entry vector containing no receptor gene (empty vector).

Figure S4

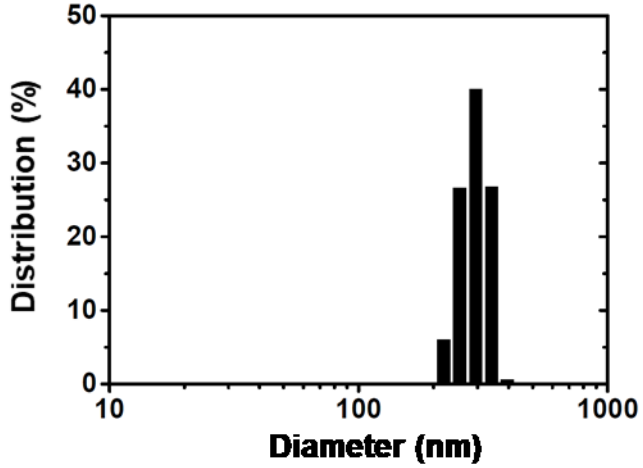

Figure S4. Dynamic light scattering (DLS) measurement of nanovesicles containing $GABA_A$ receptors.

Figure S5

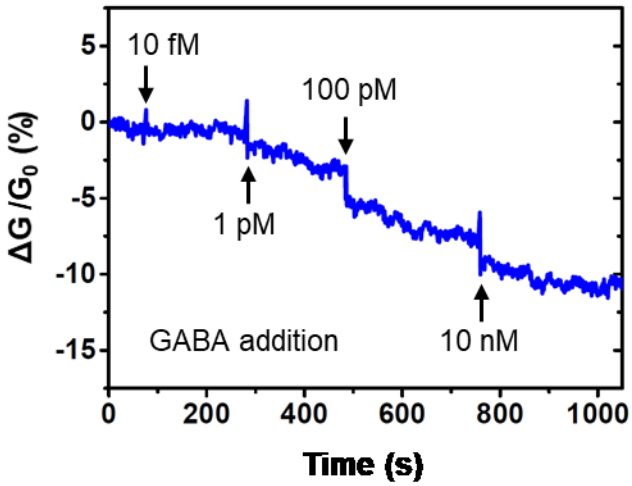

Figure S5. Real-time responses of a CNT-FET hybrid device with $GABA_A$-receptor subunits of α1β2γ2 to the addition of GABA solutions. The CNT channel conductance decreased with increasing GABA concentrations.

Figure S6

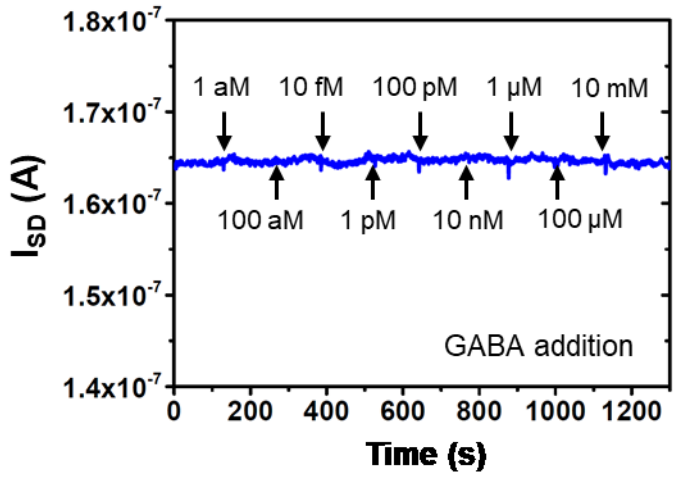

Figure S6. Real-time responses of a CNT-FET hybrid device with mock nanovesicles to the addition of GABA solutions. The CNT channel conductance remained constant while the GABA concentration increased.

Figure S7

Comparison of different methods for GABA detection

Analytical method	Limit of detection (M)	Recognition element	Reference
HPLC with electrochemical detection	9.7×10^{-7}	Electroactive derivatives for GABA labeling	Monge-Acuña and Fornaguera-Trías, 2009
Piezoelectric immunosensor	4.2×10^{-5}	GABA antibody	Wang and Muthuswamy, 2008
Differential pulse voltammetry	2.7×10^{-9}	Molecularly imprinted polymer	Prasad et al. 2013
Amperometry	2.0×10^{-6}	GABase enzyme	Hossain et al. 2018
Surface-enhanced Raman spectroscopy	1.16×10^{-7}	polypyrrole-coated Au nanoparticle	El-Said et al. 2020
Localized surface plasmon resonance	10^{-15}	mesoporous SiO_2 core–shell nanosphere	Huang et al. 2017
Antibody-based field-effect transistor	9.7×10^{-13}	GABA antibody	Lee et al. 2019
Nanovesicle-based field-effect transistor	1.0×10^{-18}	$GABA_A$ receptor	This work

Figure S7. Comparison of LODs among different methods for GABA detection with various recognition elements.

Figure S8

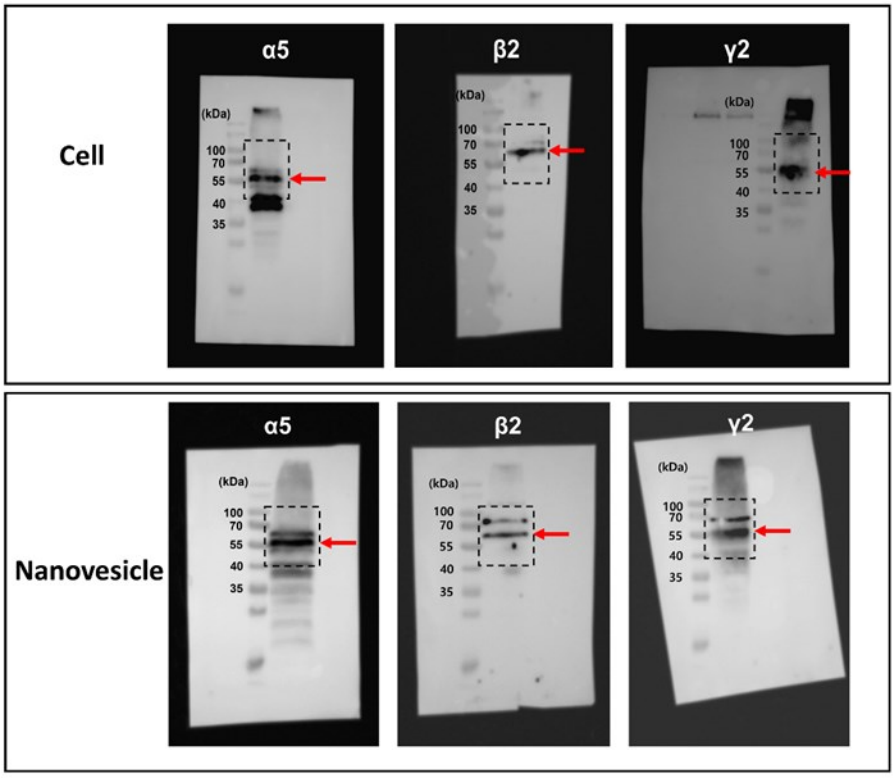

Figure S8. Full-length western blot bands corresponding to Figure 2a. Black dashed lines represent the cropping areas.

Figure S9

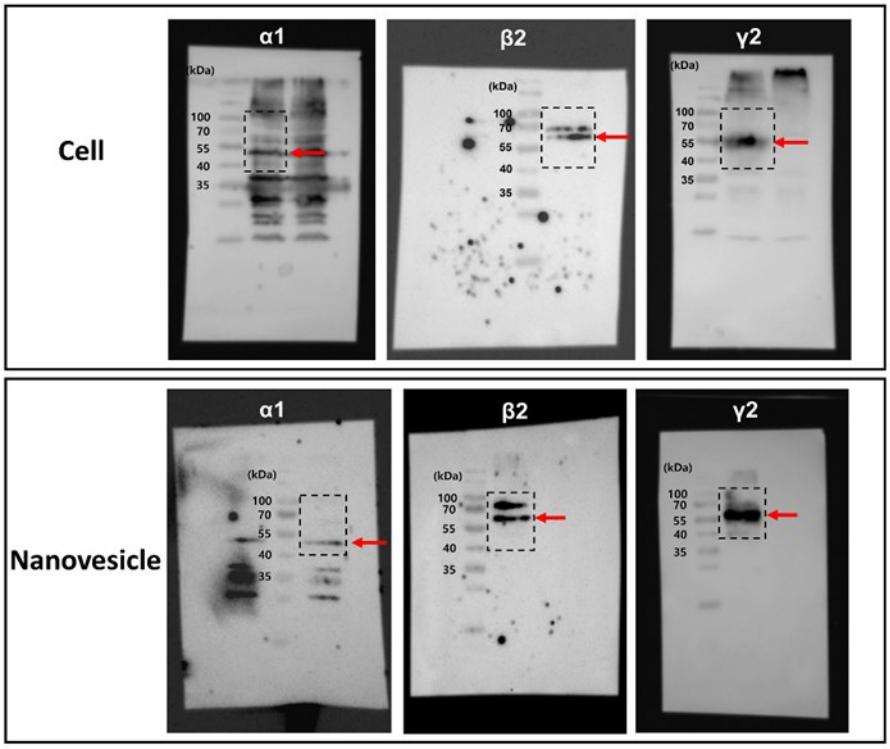

Figure S9. Full-length western blot bands corresponding to Figure S2a. Black dashed lines represent the cropping areas.